*American Mineralogist, Volume 82, pages 936–945, 1997*

# Clintonite-1*M*: Crystal chemistry and its relationships to closely associated Al-rich phlogopite

**Elisa Alietti, Maria Franca Brigatti, and Luciano Poppi**

Dipartimento di Scienze della Terra, Università Degli Studi di Modena, Via S. Eufemia, 19, I-41100, Modena, Italy

## Abstract

Crystal-structure refinements were performed on clintonite-1*M* crystals [ideal composition $^{[6]}Ca^{[6]}(Mg_2Al)^{[4]}(SiAl_3)O_{10}(OH)_2$] from skarns of the Predazzo-Monzoni area and Adamello Massif (northern Italy) with the aim of characterizing some aspects of their crystal chemistry and their relationships with closely associated phlogopite-1*M*. In the clintonite samples examined, the tetrahedral composition ranges from $Si_{1.19}Al_{2.78}Fe_{0.03}$ to $Si_{1.28}Al_{2.70}Fe_{0.02}$, indicating that the extent of the exchange vector $^{[4]}Al_{-1}{}^{[6]}Mg_{-2}{}^{[4]}Si^{[6]}(Al,\square)$, which links trioctahedral with dioctahedral Ca-bearing brittle micas, was very limited. Single-crystal X-ray diffraction data were collected and structure refinements completed in space group *C2/m* converging to $R_{obs}$ from 0.027 to 0.037 for six samples. The $^{[4]}Al^{3+}$ for $^{[4]}Si^{4+}$ substitution, which is close to 70%, produces more regular and flatter tetrahedra than in the case of phlogopite, together with an increase in the thickness and in the lateral dimensions of the sheet; the presence of $Al^{3+}$ in octahedral coordination, on the other hand, reduces the dimensions of both M1 and M2 sites with a consequent decrease in the thickness of the sheet. The volume, the flattening angle $\Psi$, and the central cation off-center shift (BLD) of the trans M1 octahedral site are greater than those of the cis M2 site, thus indicating a normal octahedral ordering. The high misfit value (from 1.187 to 1.326 Å) between tetrahedral and octahedral sheets is mostly compensated by the distortion of the tetrahedral ring (tetrahedral rotation angle $\alpha$: $23.1 \leq \alpha \leq 24.9°$). Relative to phlogopite, the interlayer separation in clintonite is reduced by about 0.6 Å.

## Introduction

The trioctahedral brittle mica clintonite, ideally $^{[6]}Ca^{[6]}(Mg_2Al)^{[4]}(SiAl_3)O_{10}(OH)_2$ in composition, is not very common, but it is of mineralogical and petrological interest. Clintonite has a high $Al^{3+}$ content, which violates the aluminium-avoidance principle of Loewenstein (1954), and it has important petrogenetic implications for thermally metamorphosed Ca- and Al-rich and Si-poor rocks (Olesch 1975; Olesch and Seifert 1976; Bucher-Nurminen 1976). The formation of clintonite in natural environments appears to be a function of both bulk rock composition and $CO_2$ ($a_{CO_2}$) and potassium ($a_{KO_{1/2}}$) activities, which must be low. An increase in $a_{KO_{1/2}}$ leads to clintonite-phlogopite assemblages (Bucher-Nurminen 1976).

In an experimental study (Olesch 1975), it was reported that the field of homogeneous clintonite at constant $H_2O$ pressure ($P_{H_2O}$ = 2 kbar) occurs at temperatures up to 870 °C and that the tetrahedral Si/Al ratio varies between 0.18 and 0.54. However, these relationships are not straightforward because the $^{[4]}Al^{3+}$ for $^{[4]}Si^{4+}$ substitution is heterovalent and involves other heterovalent substitutions in the structure to maintain electroneutrality. The primary exchange component in clintonite is $^{[4]}Si_{-1}{}^{[6]}Mg_{-1}{}^{[4]}Al^{[6]}Al$, requiring $Al^{3+}$ substitution in both tetrahedral and octahedral sites.

The X-ray structure and the crystal chemical complexity of natural clintonites was reviewed by MacKinney et al. (1988). In this paper, we explore aspects of clintonite crystal chemistry not previously treated comprehensively, such as the relationship between clintonite and closely associated phlogopite.

## Sample occurrence

The crystals examined occur in very small lenses of contact metamorphic siliceous, argillitic marbles of the Predazzo-Monzoni Hills area and of the Adamello Massif. Both localities are in the Italian Alps (northern Italy). Polished thin sections of rock were first examined on a wavelength-dispersive electron microprobe (ARL-SEMQ) and on the scanning electron microscope (Philips SEM XL40 with an EDAX energy dispersive detector) by backscattered-electron imaging and X-ray maps to test crystal homogeneity. Homogeneous clintonite crystals occur in samples Cli5a, Cli7c, Cli8a, and Cli8d from Toal de la Foja (Monzoni Hills) and in samples Cli9a and Cli9b from Farinas di Stabio (Adamello Massif), whereas in some samples from Toal de la Foja and in samples

0003–004X/97/0910–0936$05.00

**TABLE 1.** Selected structural parameters and crystal chemical formulas of the Al-rich phlogopite crystals

| | Phl1a | Phl1b | Phl2a | Phl3a | Phl4a |
|---|---|---|---|---|---|
| **Unit-cell parameters** | | | | | |
| *a* (Å) | 5.306(1) | 5.309(2) | 5.305(2) | 5.299(1) | 5.307(2) |
| *b* (Å) | 9.135(3) | 9.180(5) | 9.189(3) | 9.179(2) | 9.199(1) |
| *c* (Å) | 10.272(3) | 10.291(4) | 10.286(3) | 10.279(3) | 10.291(2) |
| β (°) | 100.01(2) | 100.00(4) | 99.96(2) | 99.90(2) | 99.89(2) |
| *V* (Å$^3$) | 493.5 | 493.9 | 493.9 | 492.5 | 494.9 |
| **Tetrahedral and interlayer parameters** | | | | | |
| ⟨T-O⟩ (Å) | 1.660 | 1.662 | 1.663 | 1.666 | 1.661 |
| ⟨T-O⟩$_{basal}$ (Å) | 1.657 | 1.661 | 1.662 | 1.663 | 1.663 |
| T-O3 (Å) | 1.667(2) | 1.663(2) | 1.665(2) | 1.673(3) | 1.656(2) |
| *V* (Å$^3$) | 2.346 | 2.355 | 2.359 | 2.371 | 2.352 |
| α (°) | 10.2 | 10.7 | 11.1 | 12.5 | 10.7 |
| τ (°) | 110.1(1) | 110.3(1) | 110.1(1) | 109.6(1) | 110.3(1) |
| TAV (°)$^2$ | 0.48 | 0.89 | 0.51 | 0.03 | 0.91 |
| BLD$_T$ (%) | 0.261 | 0.086 | 0.096 | 0.210 | 0.226 |
| ELD$_T$ (%) | 0.515 | 0.551 | 0.439 | 0.221 | 0.418 |
| Sheet thickness (Å) | 2.253 | 2.257 | 2.259 | 2.250 | 2.254 |
| Interlayer separation (Å) | 3.480 | 3.487 | 3.484 | 3.515 | 3.481 |
| **Octahedral parameters** | | | | | |
| ⟨M1-O⟩ (Å) | 2.066 | 2.066 | 2.067 | 2.067 | 2.072 |
| ⟨M2-O⟩ (Å) | 2.065 | 2.065 | 2.064 | 2.066 | 2.070 |
| $V_{M1}$ (Å$^3$) | 11.561 | 11.576 | 11.571 | 11.542 | 11.668 |
| $V_{M2}$ (Å$^3$) | 11.536 | 11.556 | 11.514 | 11.351 | 11.644 |
| BLD$_{M1}$ (%) | 0.644 | 0.639 | 0.658 | 0.553 | 0.600 |
| BLD$_{M2}$ (%) | 0.260 | 0.383 | 0.305 | 0.326 | 0.514 |
| ELD$_{M1}$ (%) | 5.095 | 4.999 | 5.116 | 5.435 | 4.845 |
| ELD$_{M2}$ (%) | 5.061 | 4.970 | 5.041 | 5.190 | 4.816 |
| ψ$_{M1}$ (°) | 58.99 | 58.92 | 59.00 | 59.28 | 58.75 |
| ψ$_{M2}$ (°) | 58.97 | 58.89 | 58.93 | 59.06 | 58.74 |
| $e_u/e_{sM1}$ | 1.1074 | 1.1053 | 1.1077 | 1.1147 | 1.1016 |
| $e_u/e_{sM2}$ | 1.1068 | 1.1047 | 1.1062 | 1.1095 | 1.1011 |
| OAV$_{M1}$ (°)$^2$ | 37.22 | 35.95 | 37.87 | 42.55 | 33.67 |
| OAV$_{M2}$ (°)$^2$ | 37.10 | 35.95 | 37.42 | 39.55 | 34.12 |
| Sheet thickness (Å) | 2.129 | 2.134 | 2.130 | 2.112 | 2.149 |
| Δ$_{TM}$ (Å) | 0.580 | 0.585 | 0.606 | 0.668 | 0.574 |
| **Crystal chemical formulas** | | | | | |
| Phl1a | $^{[4]}(Si_{2.74}Al_{1.26})^{[6]}(Al_{0.24}Fe^{3+}_{0.09}Fe^{2+}_{0.12}Mg_{2.48}Mn_{0.01}Ti_{0.02})^{[12]}(Na_{0.04}K_{0.93})O_{9.99}[(OH)_{1.95}F_{0.06}]$ | | | | |
| Phl1b | $^{[4]}(Si_{2.65}Al_{1.35})^{[6]}(Al_{0.24}Fe^{3+}_{0.07}Fe^{2+}_{0.11}Mg_{2.55}Mn_{0.01}Ti_{0.02})^{[12]}(Na_{0.04}K_{0.93})O_{9.96}[(OH)_{1.95}F_{0.09}]$ | | | | |
| Phl2a | $^{[4]}(Si_{2.60}Al_{1.40})^{[6]}(Al_{0.18}Fe^{3+}_{0.15}Fe^{2+}_{0.03}Mg_{2.63}Ti_{0.01})^{[12]}(Na_{0.02}K_{0.95}Ba_{0.01})O_{9.93}[(OH)_{1.96}F_{0.11}]$ | | | | |
| Phl3a | $^{[4]}(Si_{2.50}Al_{1.50})^{[6]}(Al_{0.47}Fe^{3+}_{0.15}Fe^{2+}_{0.07}Mg_{2.23}Mn_{0.04}Ti_{0.01})^{[12]}(Na_{0.02}K_{0.95}Ba_{0.01})O_{10.02}[(OH)_{1.94}F_{0.04}]$ | | | | |
| Phl4a | $^{[4]}(Si_{2.60}Al_{1.40})^{[6]}(Al_{0.20}Fe^{3+}_{0.11}Fe^{2+}_{0.04}Mg_{2.64}Mn_{0.01})^{[12]}(Na_{0.02}K_{0.90}Ca_{0.02}Ba_{0.02})O_{9.92}[(OH)_{2.02}F_{0.06}]$ | | | | |

*Note:* The definitions of the different parameters are reported in the footnote of Table 6.

from Toal del Mason (Monzoni Hills) X-ray maps of some mica crystals, polished parallel to [001] show two sets of distinct layers perpendicular to (001) whose composition corresponds to phlogopite and clintonite, respectively (Alietti 1996). These samples were not investigated further.

In samples Cli5a, Cli7c, Cli8a, and Cli8d clintonite occurs as a major green to dark-green replacement mineral in addition to spinel, fassaite, and calcite (Morandi et al. 1984). In samples Cli9a and Cli9b clintonite crystals occur as coarse, dark-green flakes with fassaitic pyroxene, olivine, calcite, spinel, chlorite, and andraditic garnet (Ulmer 1982).

Crystal chemical data on phlogopite crystals (referred to as Al-rich phlogopite: Phl1a, Phl1b, Phl2a, Phl3a, and Phl4a) have been published previously by Alietti et al. (1995) and are summarized in Table 1. Compared to the ideal phlogopite composition $^{[12]}K^{[6]}Mg_3{}^{[4]}(Si_3Al)O_{10}(OH)_2$ these crystals exhibit a large degree of $^{[4]}Al^{3+}$ for $^{[4]}Si^{4+}$ substitution, which is compensated primarily by $^{[6]}Al^{3+}$ (and or $^{[6]}Fe^{3+}$) for $^{[6]}Mg^{2+}$ substitutions (exchange vector $^{[4]}Si_{-1}{}^{[6]}Mg_{-1}{}^{[4]}Al^{[6]}Al$).

## ANALYTICAL METHODS

### Chemical analysis

The compositions of clintonite crystals were determined using an ARL-SEMQ wavelength-dispersive electron microprobe. Polished thin sections from about 30 rock samples and the crystals used for structure refinements were analyzed (Table 2). A minimum of 20 mica crystals were analyzed in each section, multiple point analyses being performed for each crystal to test for chemical homogeneity.

The variation in the composition of individual crystals selected for X-ray study was below 3% for $Mg^{2+}$, $Al^{3+}$, $Si^{4+}$, and $Ca^{2+}$ and typically below 2%. Accordingly, six to ten spot analyses were averaged to obtain the data in Table 2. No systematic chemical zoning was observed in crystals from the same rock sample.

**TABLE 2.** Averaged chemical composition, structural formulas, mean atomic number of octahedral and interlayer sites, and Al in tetrahedral sites

| | Cli5a | Cli7c | Cli8a | Cli8d | Cli9a | Cli9b |
|---|---|---|---|---|---|---|
| **Oxide (wt%)** | | | | | | |
| $SiO_2$ | 17.05 | 16.74 | 17.84 | 17.60 | 16.87 | 18.08 |
| $TiO_2$ | 0.07 | 0.06 | 0.05 | 0.07 | 0.13 | 0.20 |
| $Al_2O_3$ | 41.38 | 41.00 | 42.31 | 40.98 | 41.31 | 40.10 |
| $Fe_2O_3$ | 0.66 | 0.33 | b.d.t. | b.d.t. | 0.50 | 0.41 |
| FeO | 1.79 | 3.70 | 2.47 | 2.29 | 2.65 | 2.65 |
| MgO | 20.98 | 20.21 | 19.91 | 21.09 | 20.57 | 20.89 |
| MnO | 0.05 | b.d.t. | b.d.t. | b.d.t. | b.d.t. | b.d.t. |
| CaO | 13.04 | 13.00 | 12.64 | 12.85 | 12.88 | 12.55 |
| BaO | 0.05 | b.d.t. | b.d.t. | b.d.t. | b.d.t. | b.d.t. |
| $Na_2O$ | 0.10 | 0.10 | 0.14 | 0.15 | 0.03 | 0.10 |
| $K_2O$ | 0.01 | b.d.t. | 0.01 | b.d.t. | 0.01 | b.d.t. |
| $H_2O$ | 4.20 | 4.38 | 4.20 | 4.20 | 4.20 | 4.20 |
| F | 0.63 | 0.48 | 0.42 | 0.77 | 0.85 | 0.83 |
| Sum | 100.01 | 100.00 | 99.99 | 100.00 | 100.00 | 100.01 |
| **Structural formulas (apfu)** | | | | | | |
| Si | 1.20 | 1.19 | 1.25 | 1.24 | 1.19 | 1.28 |
| Al | 2.76 | 2.79 | 2.75 | 2.76 | 2.78 | 2.70 |
| $Fe^{3+}$ | 0.04 | 0.02 | — | — | 0.03 | 0.02 |
| Sum | 4.00 | 4.00 | 4.00 | 4.00 | 4.00 | 4.00 |
| Al | 0.68 | 0.64 | 0.76 | 0.65 | 0.67 | 0.63 |
| $Fe^{2+}$ | 0.11 | 0.22 | 0.15 | 0.13 | 0.16 | 0.16 |
| Mg | 2.21 | 2.14 | 2.09 | 2.22 | 2.17 | 2.20 |
| Ti | — | — | — | — | 0.01 | 0.01 |
| Sum | 3.00 | 3.00 | 3.00 | 3.00 | 3.01 | 3.00 |
| Na | 0.01 | 0.01 | 0.02 | 0.02 | — | 0.01 |
| Ca | 0.99 | 0.99 | 0.95 | 0.97 | 0.98 | 0.95 |
| Sum | 1.00 | 1.00 | 0.97 | 0.99 | 0.98 | 0.96 |
| OH | 1.98 | 2.07 | 1.97 | 1.97 | 1.98 | 1.98 |
| F | 0.14 | 0.11 | 0.09 | 0.17 | 0.19 | 0.18 |
| O | 9.88 | 9.82 | 9.94 | 9.86 | 9.83 | 9.84 |
| Sum | 12.00 | 12.00 | 12.00 | 12.00 | 12.00 | 12.00 |
| **Mean atomic number ($e^-$)** | | | | | | |
| $M1_{Xref}$ | 13.0(1) | 13.4(1) | 13.2(1) | 12.7(1) | 13.0(1) | 12.6(1) |
| $M2_{Xref}$ | 12.6(1) | 13.3(1) | 12.9(1) | 13.0(1) | 13.1(1) | 13.0(1) |
| $(M1 + 2M2)_{Xref}$ | 38.2 | 40.0 | 39.0 | 38.7 | 39.2 | 38.6 |
| $(M1 + M2)_{EPMA}$ | 38.2 | 39.7 | 38.9 | 38.5 | 39.1 | 39.0 |
| $A_{Xref}$ | 19.8(1) | 19.8(1) | 19.1(1) | 19.4(1) | 19.4(1) | 19.1(1) |
| $A_{EPMA}$ | 19.9 | 19.9 | 19.2 | 19.6 | 19.6 | 19.1 |
| **Tetrahedral Al occupancies (%)** | | | | | | |
| Xref* | 71.6 | 78.2 | 73.5 | 73.9 | 79.5 | 69.3 |
| EPMA | 70.0 | 70.3 | 68.8 | 69.0 | 70.2 | 68.0 |

*Note:* Xref = X-ray refinement; EPMA = electron microprobe; b.d.t. = below detection threshold.

* Following the algorithms of Alberti and Gottardi (1988).

The F determination was obtained following the procedures of Foley (1989); Cl was below the detection limit. X-ray counts were converted into oxide weight percentages using the $\varphi(\rho Z)$ algorithm of Pouchou and Pichoir (1991).

Analyses of $(OH)^-$ and $Fe^{2+}$ were performed on crystals taken from the same sample from which the crystal was taken for structure refinement; $(OH)^-$ was determined by thermogravimetric analysis in Ar gas to prevent Fe oxidation (Seiko 5200 thermal analyzer; heating rate of 10 °C/min; flow rate 200 mL/min), and $Fe^{2+}$ by a semimicrovolumetric method (Meyrowitz 1970). The structural formulas (Table 2) were calculated on $O_{12-x-y}$-$2OHxFy$. The $Fe^{3+}$ was assigned to the tetrahedral site following the suggestion of Annersten and Olesch (1978), Joswig et al. (1986), and MacKinney et al. (1988), on the basis of Mössbauer spectra results. These authors indicated a strong preference for the tetrahedral site of $Fe^{3+}$ over $Al^{3+}$ owing to clintonite's large tetrahedral site.

## Single-crystal X-ray data collection and structure refinement

Most crystals selected from rock samples that did not display zoning were extracted by crushing and grinding small fragments. In general, crystal quality was low and in some cases [310] twinning or polytype mixtures ($1M + 1M_d$ and $1M + 2M_1$) were present. These features were determined by a precession or Weissenberg photograph and transmission electron microscopy. Crystals were selected by precession methods for cell dimension and intensity data despite streaking due to reflections in the ω direction in the low-θ region. For the six crystals selected, the absence of $h + k \neq 2n$ reflections confirmed the *C*-centered unit cell, whereas the intensity distribution along rows [13*l*] and [02*l*] indicated a 1*M* polytype (space group *C2/m*) (Bailey 1988).

Crystals Cli5a, Cli7c, Cli8a, Cli9a, and Cli9b were mounted on an automated CAD4 (Enraf-Nonius) single-crystal X-ray diffractometer (Mo*K*α, λ = 0.71073 Å, graphite-monochromatized radiation, operating at 52 kV and 40 mA). Cell dimensions were determined using the 2θ values for 25 centered reflections with $10° \leq \theta \leq 25°$ (Table 3). Intensities were collected in the θ range 1.5–

**TABLE 3.** Unit cell dimensions and details of the X-ray data collection and structure refinement of clintonite crystals

| Sample | Dimensions (mm) | $N_{obs}$ | $R_{sym}$ (× 100) | $R_{obs}$ (× 100) | *a* (Å) | *b* (Å) | *c* (Å) | β (°) | *V* (Å³) |
|---|---|---|---|---|---|---|---|---|---|
| Cli5a | 0.21 × 0.12 × 0.03 | 620 | 2.25 | 3.49 | 5.200(1) | 9.005(2) | 9.795(2) | 100.24(2) | 451.4 |
| Cli7c | 0.32 × 0.27 × 0.03 | 536 | 1.12 | 3.73 | 5.198(1) | 9.006(1) | 9.796(1) | 100.21(1) | 451.3 |
| Cli8a | 0.18 × 0.09 × 0.03 | 568 | 2.20 | 3.11 | 5.194(1) | 8.995(2) | 9.788(2) | 100.23(2) | 450.0 |
| Cli8d | 0.18 × 0.09 × 0.02 | 499 | 2.60 | 3.18 | 5.203(1) | 9.026(2) | 9.811(1) | 100.27(1) | 453.4 |
| Cli9a | 0.48 × 0.42 × 0.04 | 513 | 1.92 | 3.29 | 5.192(2) | 9.003(2) | 9.794(2) | 100.17(2) | 450.6 |
| Cli9b | 0.27 × 0.06 × 0.03 | 493 | 1.75 | 2.70 | 5.202(1) | 9.005(2) | 9.816(2) | 100.30(1) | 452.4 |

*Note:* $R_{sym} = \frac{\sum_{hkl}\sum_{i=1}^{N}|I_{hkl_i} - I_{hkl}|}{\sum_{hkl}\sum_{i=1}^{N}I_{hkl}}$.

**TABLE 5.** Selected bond lengths (Å) from structure refinement of clintonite crystals

| | Cli5a | Cli7c | Cli8a | Cli8d | Cli9a | Cli9b |
|---|---|---|---|---|---|---|
| T-O1 | 1.733(2) | 1.743(2) | 1.736(2) | 1.737(2) | 1.751(2) | 1.728(2) |
| T-O2 | 1.733(2) | 1.746(2) | 1.735(2) | 1.737(2) | 1.736(3) | 1.728(2) |
| T-O2′ | 1.732(2) | 1.745(3) | 1.739(2) | 1.734(2) | 1.756(3) | 1.730(2) |
| T-O3 | 1.727(2) | 1.732(2) | 1.720(2) | 1.733(2) | 1.751(2) | 1.714(2) |
| ⟨T-O⟩ | 1.731 | 1.742 | 1.732 | 1.735 | 1.749 | 1.725 |
| M1-O3 × 4 | 2.046(2) | 2.035(2) | 2.046(2) | 2.048(2) | 2.032(2) | 2.059(2) |
| M1-O4 × 2 | 2.011(3) | 2.021(3) | 2.008(3) | 2.016(3) | 2.023(4) | 2.009(3) |
| ⟨M1-O⟩ | 2.034 | 2.030 | 2.033 | 2.037 | 2.029 | 2.042 |
| M2-O3 × 2 | 2.008(2) | 2.012(3) | 2.010(2) | 2.009(2) | 2.006(3) | 2.009(2) |
| M2-O3′ × 2 | 2.031(2) | 2.034(2) | 2.033(2) | 2.030(2) | 2.015(2) | 2.040(2) |
| M2-O4 × 2 | 2.022(2) | 2.034(3) | 2.027(2) | 2.028(2) | 2.052(3) | 2.014(2) |
| ⟨M2-O⟩ | 2.020 | 2.027 | 2.023 | 2.022 | 2.024 | 2.021 |
| A-O1 × 2 | 3.565(3) | 3.580(4) | 3.573(3) | 3.570(4) | 3.618(4) | 3.554(3) |
| A-O1′ × 2 | 2.432(3) | 2.410(4) | 2.421(3) | 2.433(3) | 2.399(4) | 2.449(3) |
| A-O2 × 4 | 3.559(2) | 3.588(3) | 3.571(2) | 3.560(2) | 3.595(3) | 3.554(2) |
| A-O2′ × 4 | 2.432(2) | 2.406(3) | 2.415(2) | 2.436(2) | 2.396(3) | 2.442(2) |
| $\langle A\text{-}O\rangle_{inner}$ | 2.432 | 2.407 | 2.417 | 2.435 | 2.397 | 2.444 |
| $\langle A\text{-}O\rangle_{outer}$ | 3.561 | 3.585 | 3.572 | 3.563 | 3.603 | 3.554 |
| Δ⟨A-O⟩ | 1.129 | 1.178 | 1.155 | 1.128 | 1.206 | 1.110 |

**TABLE 6.** Selected tetrahedral, octahedral, and interlayer parameters derived from structure refinements of clintonite crystals

| | Cli5a | Cli7c | Cli8a | Cli8d | Cli9a | Cli9b |
|---|---|---|---|---|---|---|
| **Tetrahedral parameters** | | | | | | |
| α (°) | 23.4 | 24.4 | 23.9 | 23.4 | 24.9 | 23.1 |
| Δz (Å) | 0.0037 | 0.0019 | 0.0070 | 0.0117 | 0.0272 | 0.0063 |
| τ (°) | 109.2(1) | 109.2(1) | 109.2(1) | 109.4(1) | 108.9(1) | 109.3(1) |
| TAV (°)² | 0.1 | 0.1 | 0.1 | 0.0 | 0.5 | 0.1 |
| TQE | 1.0000 | 1.0001 | 1.0001 | 1.0000 | 1.0001 | 1.0001 |
| $V_T$ (Å³) | 2.663 | 2.710 | 2.667 | 2.680 | 2.743 | 2.636 |
| $BLD_T$ (%) | 0.127 | 0.276 | 0.368 | 0.094 | 0.356 | 0.323 |
| $ELD_T$ (%) | 0.233 | 0.334 | 0.441 | 0.122 | 0.316 | 0.321 |
| **Octahedral parameters** | | | | | | |
| $\psi_{M1}$ (°) | 59.05 | 58.76 | 58.80 | 59.08 | 58.79 | 59.01 |
| $\psi_{M2}$ (°) | 58.81 | 58.70 | 58.63 | 58.82 | 58.71 | 58.65 |
| $e_{sM1}$ (Å) | 2.7242 | 2.7293 | 2.7318 | 2.7276 | 2.7260 | 2.7363 |
| $e_{sM2}$ (Å) | 2.7136 | 2.7266 | 2.7243 | 2.7162 | 2.7226 | 2.7206 |
| $e_{uM1}$ (Å) | 3.0220 | 3.0066 | 3.0128 | 3.0273 | 3.0055 | 3.0325 |
| $e_{uM2}$ (Å) | 2.9929 | 2.9992 | 2.9920 | 2.9964 | 2.9964 | 2.9890 |
| $OQE_{M1}$ | 1.0119 | 1.0101 | 1.0106 | 1.0120 | 1.0103 | 1.0119 |
| $OQE_{M2}$ | 1.0108 | 1.0100 | 1.0098 | 1.0108 | 1.0101 | 1.0103 |
| $OAV_{M1}$ (°)² | 38.7 | 33.5 | 34.4 | 39.0 | 34.1 | 38.25 |
| $OAV_{M2}$ (°)² | 35.7 | 32.9 | 32.5 | 35.7 | 33.0 | 34.0 |
| $V_{M1}$ (Å³) | 11.028 | 10.992 | 11.037 | 11.077 | 10.964 | 11.159 |
| $V_{M2}$ (Å³) | 10.817 | 10.937 | 10.885 | 10.852 | 10.896 | 10.840 |
| $BLD_{M1}$ (%) | 0.768 | 0.294 | 0.829 | 0.689 | 0.204 | 1.097 |
| $BLD_{M2}$ (%) | 0.401 | 0.469 | 0.446 | 0.435 | 0.914 | 0.632 |
| $ELD_{M1}$ (%) | 5.183 | 4.834 | 4.891 | 5.208 | 4.877 | 5.134 |
| $ELD_{M2}$ (%) | 4.895 | 4.760 | 4.683 | 4.868 | 4.787 | 4.701 |
| **Sheet thickness** | | | | | | |
| Tetrahedral (Å) | 2.319 | 2.316 | 2.309 | 2.329 | 2.311 | 2.317 |
| Octahedral (Å) | 2.092 | 2.106 | 2.107 | 2.094 | 2.102 | 2.103 |
| Interlayer (Å) | 2.909 | 2.902 | 2.908 | 2.902 | 2.916 | 2.921 |
| $\Delta_{TM}$ (Å) | 1.225 | 1.280 | 1.244 | 1.224 | 1.326 | 1.187 |

*Notes:* α (tetrahedral rotation angle) = $\Sigma_{i=1}^{6}\alpha_i/6$ where $\alpha_i = |120° - \phi_i|/2$ and where $\phi_i$ is the angle between basal edges of neighboring tetrahedra articulated in the ring. $\Delta z = [Z_{(O_{basal})max} - Z_{(O_{basal})min}]$ [c sin β]. τ (tetrahedral flattening angle) = $\Sigma_{i=1}^{3}(O_{basal} - \hat{T} - O_{basal})_i/3$. TAV (tetrahedral angle variance) = $\Sigma_{i=1}^{6}(\theta_i - 109.47)^2/5$ (Robinson et al. 1971). TQE (tetrahedral quadratic elongation) = $\Sigma_{i=1}^{4}(l_i/l_0)^2/4$ where $l_0$ is the center to vertex distance for an undistorted tetrahedron whose volume is equal to that of the distorted tetrahedron with bond length $l_i$ (Robinson et al. 1971). ψ (octahedral flattening angle) = $\cos^{-1}$[octahedral thickness/(2⟨M-O⟩)] (Donnay et al. 1964). $e_u$, $e_s$ = mean lengths of unshared and shared edges, respectively (Toraya 1981). OQE (octahedral quadratic elongation) $\Sigma_{i=1}^{6}(l_i/l_0)^2/6$ where $l_0$ is the center to vertex distance for an undistorted octahedron whose volume is equal to that of the distorted octahedron with bond length $l_i$ (Robinson et al. 1971). OAV (octahedral angle variance) = $\Sigma_{i=1}^{12}(\theta_i - 90°)^2/11$ (Robinson et al. 1971).

$$\text{BLD} = \text{(bond length distortion)}\ \frac{100}{n}\Sigma_{i=1}^{n}\frac{|(X - O)_i - (\langle X - O\rangle)|}{(\langle X - O\rangle)}\%$$

where $n$ is the number of bonds and ($X$−O) the central cation − oxygen length (Renner and Lehmann 1986).

$$\text{ELD} = \text{(edge length distortion)}\ \frac{100}{n}\Sigma_{i=1}^{n}\frac{|(O - O)_i - (\langle O - O\rangle)|}{(\langle O\text{-}O\rangle)}\%$$

where $n$ is the number of bonds and (O-O) the polyedron edge length (Renner and Lehmann 1986). $\Delta_{TM}$ (dimensional misfit) = $2\sqrt{3}\,\langle O\text{-}O\rangle_{basal} - 3\sqrt{2}$ (2⟨M2-O⟩ + ⟨M1-O⟩)/3 (Toraya 1981).

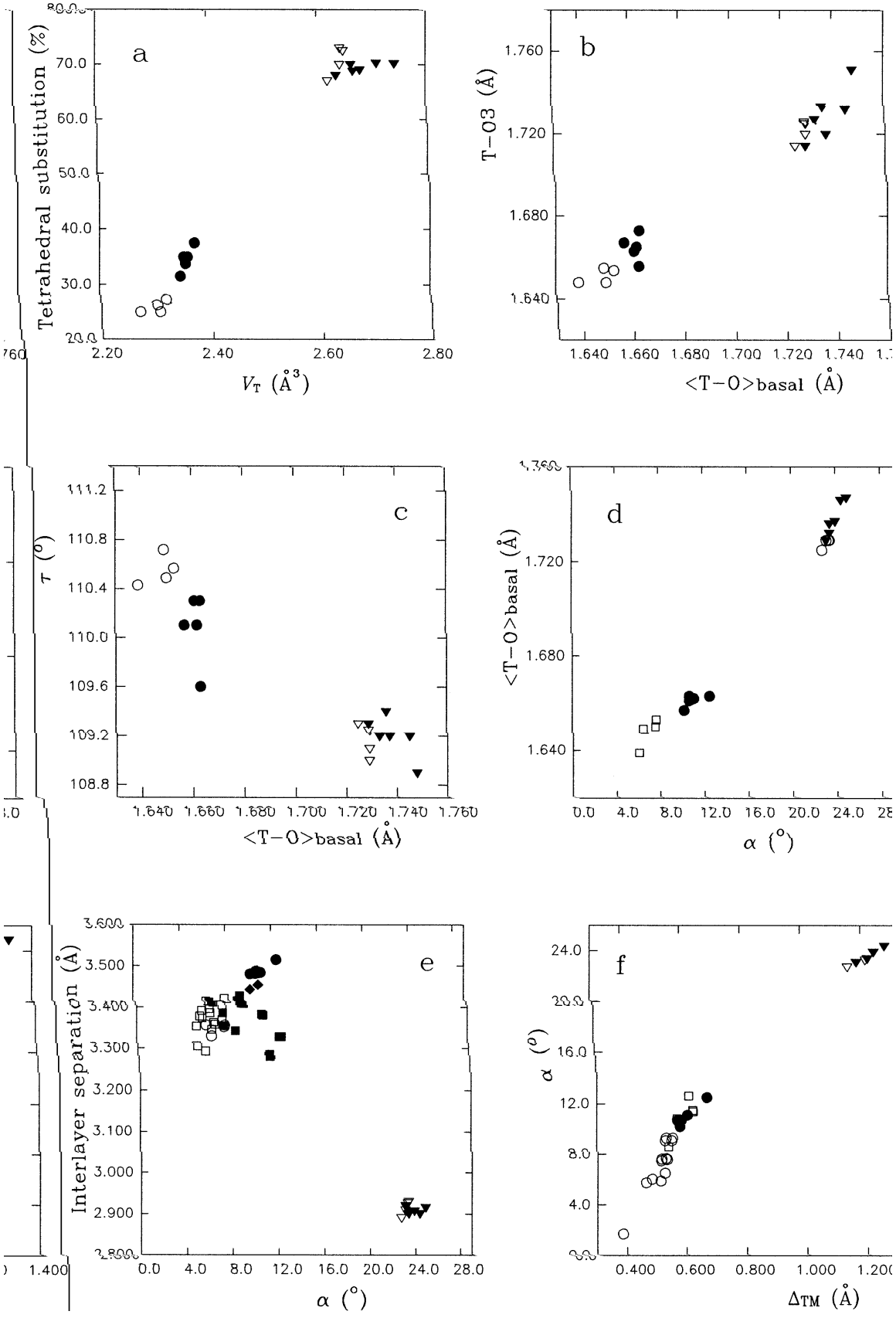
a
Tetrahedral substitution (%)
70.0
60.0
50.0
40.0
30.0
20.0
2.20
2.40
2.60
2.80
$V_T$ (Å$^3$)
b
T–O3 (Å)
1.760
1.720
1.680
1.640
1.640 1.660 1.680 1.700 1.720 1.740
<T–O>basal (Å)
c
τ (°)
111.2
110.8
110.4
110.0
109.6
109.2
108.8
1.640 1.660 1.680 1.700 1.720 1.740 1.760
<T–O>basal (Å)
d
<T–O>basal (Å)
1.720
1.680
1.640
0.0 4.0 8.0 12.0 16.0 20.0 24.0
α (°)
e
Interlayer separation (Å)
3.500
3.400
3.300
3.200
3.100
3.000
2.900
0.0 4.0 8.0 12.0 16.0 20.0 24.0 28.0
α (°)
f
α (°)
24.0
16.0
12.0
8.0
4.0
0.400 0.600 0.800 1.000
$\Delta_{TM}$ (Å)

35° ($-1 \le h \le 8$; $-14 \le k \le 14$; $-15 \le l \le 15$) using the ω scan mode (scan rate 1°/min; scan window 2–4°).

The unit-cell parameters and intensity data of crystal Cli8d were obtained using a Siemens rotating-anode automated four-circle X-ray diffractometer (Mo$K\alpha$ graphite monochromatized radiation, $\lambda = 0.71073$ Å, operating at 52 kV, 140 mA) and X-SCANS software (Siemens 1993). Cell parameters were determined by least-squares refinement of 40 medium-high angle reflections. Intensities were collected in the 2θ range 3–60° ($-1 \le h \le 7$; $-12 \le k \le 12$; $-13 \le l \le 13$), using the ω scan mode and a window width of 1.7°. For all crystals, X-ray intensity data were corrected for Lorentz and polarization effects and for absorption using Ψ scans (North et al. 1968). The intensity data of symmetrically equivalent reflections were averaged, the resulting discrepancy factor ($R_{sym}$) being in the range $0.011 \le R_{sym} \le 0.026$ (Table 3).

The structure refinements used a full-matrix least-squares procedure; reflections with $I \ge 5\ \sigma_I$ (Ungaretti 1980; Ungaretti et al. 1983) were used with the ORFLS program (Busing et al. 1962) and starting with positional and displacement parameters of Ertsberg clintonite (MacKinney et al. 1988) in the space group *C2/m*. The mean atomic number at each site (Table 2) were determined by assigning two scattering curves $f_1$ and $f_2$, and refining the occupancy factor *xf* with the constraint ($xf_1 + xf_2 = 1$). The atomic scattering curves were taken from the *International Tables for X-ray Crystallography* (Ibers and Hamilton 1974) and from Tokonami (1965). Fully ionized scattering factors were used for the nontetrahedral cations, whereas both neutral and ionized scattering factors were used for tetrahedral and anion sites (Brigatti and Davoli 1990). The starting scattering factors were a composite of 50% $Al^{3+}$ and 50% $Mg^{2+}$ vs. $Fe^{2+}$ for M1 sites, $Al^{3+}$ vs. $Mg^{2+}$ for M2 sites, $Ca^{2+}$ for the interlayer site, O vs. $O^{2-}$ for the anion sites and a composite of 50% Si and 50% Al vs. 50% $Si^{4+}$ and 50% $Al^{3+}$ for the tetrahedral sites. In the last phase of anisotropic refinement, scattering curves appropriate to the composition were applied and, at the final step, a difference-Fourier (Δ*F*) synthesis was calculated. The standard deviation of the Δ*F* peak, using the equation of Lipson and Cochran (1953), ranged from 0.04 to 0.09 e/Å$^3$.

Examination of the final Δ*F* map for samples Cli5a, Cli8a, Cli9a, and Cli9b showed a peak above background (≥3σ), indicating a reasonable O-H bond length (0.86–0.94 Å), located in the proximity of the O4 atom (atomic coordinates $x/a \cong 0.08$; $y/b \cong 0.52$; $z/c \cong 0.30$; peak heights 0.8–0.9 e/Å$^3$), which shows that the OH vector is nearly parallel to *c**.

Because of the relatively high discrepancy factor ($R_{obs} = 0.037$) for crystal Cli7c, structural refinement in the non-centrosymmetric *C2* and *Cm* space groups was attempted using reflections with $I \ge 2\ \sigma_I$ (Schomaker and Marsh 1979). However, as suggested by Marsh (1986) we report the structure refinement in the centrosymmetric space group because the results do not indicate clearly the ordering between $Si^{4+}$ and $Al^{3+}$ cations, or between $(OH)^-$ and $F^-$ anions.

Crystallographic coordinates and displacement parameters are listed in Table 4[1]; relevant bond distances are shown in Table 5; selected tetrahedral, octahedral and interlayer parameters are reported in Table 6, and mean atomic numbers of cation sites, as estimated by structure refinements (Xref) and electron probe microanalyses (EPMA), are reported and compared in Table 2. Observed and calculated structure factors are given in Table 7[1].

## Chemical variations

The clintonite samples examined (Table 2) have a remarkably consistent composition with few substitutions outside the $CaO$-$MgO$-$Al_2O_3$-$SiO_2$ system; the $K_2O$ + $Na_2O$ + BaO totals are below 0.16 wt% (0.02 apfu). The main octahedral substituent is FeO, ranging from 1.79 wt% (0.11 apfu) to 3.70 wt% (0.22 apfu), while the tetrahedral composition ranges from $Si_{1.19}Al_{2.78}Fe_{0.03}$ to $Si_{1.28}Al_{2.70}Fe_{0.02}$. These Al,Si limits approach the ideal $SiAl_3$ ratio and agree with those expected for natural clintonite (Takéuchi and Sadanaga 1959; 1966; Guggenheim 1984; Joswig et al. 1986; MacKinney et al. 1988). These results indicate that the extent of the exchange vector $^{[4]}Al_{-1}{}^{[6]}Mg_{-2}{}^{[4]}Si\ ^{[6]}(Al,\square)$, which links trioctahedral with dioctahedral Ca-bearing brittle micas, was very limited. The exchange vector $^{[4]}Si_{-1}{}^{[6]}Mg_{-1}{}^{[4]}Al^{[6]}Al$ was also found to be limited for phlogopite samples from the same area. Taking into account the ideal phlogopite composition, ho-

[1] For a copy of Tables 4 and 7, order Document AM-97-647 from the Business Office, Mineralogical Society of America, 1015 Eighteenth Street NW, Suite 601, Washington, DC 20036, U.S.A. Please remit $5.00 in advance. Deposit items may also be available on the American Minerologist web site, refer to inside back cover of a current issue for web address.

←

**Figure 1.** (**a**) The percentage of tetrahedral Al for Si substitution vs. tetrahedral volume ($V_T$); (**b**) tetrahedral cation-apical oxygen bond length (T-O3) vs. the mean basal T-O ($\langle T\text{-}O\rangle_{basal}$) bond length; (**c**) tetrahedral flattening angle (τ) vs. $\langle T\text{-}O\rangle_{basal}$; (**d**) $\langle T\text{-}O\rangle_{basal}$ vs. tetrahedral ring distortion (α); (**e**) interlayer separation vs. α; (**f**) α vs. dimensional misfit between tetrahedral and octahedral sheets ($\Delta_{TM}$). Symbols: filled triangles = clintonite samples this from study; filled circles = Al-rich phlogopite from the Predazzo-Monzoni area (Alietti et al. 1995); open triangles = clintonite (Joswig et al. 1986; MacKinney et al. 1988); open circles = phlogopite (Hazen and Burnham 1973; Joswig 1972; Takeda and Morosin 1975; MacCauley et al. 1973); open squares = biotite (Brigatti and Davoli 1990; Brigatti et al. 1991; Bigi et al. 1993; Brigatti and Poppi 1993) filled squares = kinoshitalite, Ba-rich biotite and Ba-rich phlogopite (Kato et al. 1979; Guggenheim and Kato 1984; Brigatti and Poppi 1993); diamonds = ferriphlogopite (Brigatti et al. 1996).

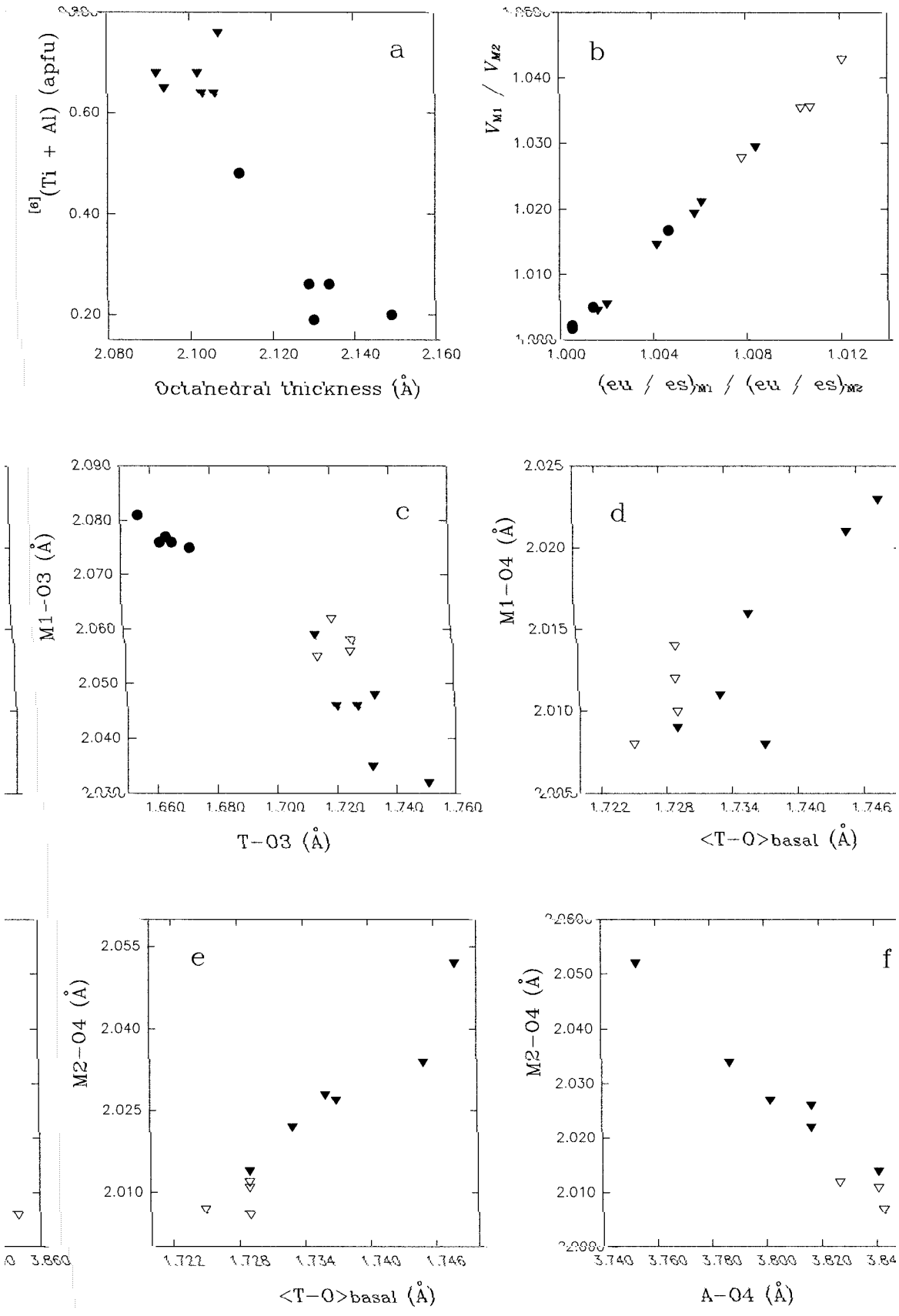
a
[6](Ti + Al) (apfu)
0.60
0.40
0.20
2.080
2.100
2.120
2.140
2.160
Octahedral thickness (Å)
b
$V_{M1}$ / $V_{M2}$
1.040
1.030
1.020
1.010
1.000
1.004
1.008
1.012
⟨eu / es⟩M1 / ⟨eu / es⟩M2
c
M1–O3 (Å)
2.090
2.080
2.070
2.060
2.050
2.040
1.660
1.680
1.700
1.720
1.740
1.760
T–O3 (Å)
d
M1–O4 (Å)
2.025
2.020
2.015
2.010
1.722
1.728
1.734
1.740
1.746
<T–O>basal (Å)
e
M2–O4 (Å)
2.055
2.040
2.025
2.010
1.722
1.728
1.734
1.740
1.746
<T–O>basal (Å)
f
M2–O4 (Å)
2.050
2.040
2.030
2.020
2.010
3.740
3.760
3.780
3.800
3.820
A–O4 (Å)

mogeneous Al-rich phlogopite crystals show that $Al^{3+}$ for $Si^{4+}$ tetrahedral substitution is mostly compensated by $Al^{3+}$ for $Mg^{2+}$ octahedral substitution. Nevertheless, the limit of $Al^{3+}$ tetrahedral substitution is below 38% of the site occupancy and agrees with the conclusions of Hewitt and Wones (1975), who stated that in synthetic phlogopite $Al^{3+}$ occupancy does not exceed 45% (Table 1). The exchange vector $^{[12]}K_{-1}{}^{[4]}Si_{-1}{}^{[6]}Ca^{[4]}Al$ is unlikely both in phlogopite and in clintonite.

## Crystal structure and crystal chemistry

### Tetrahedral sheet and interlayer sites

In the clintonite samples examined, $^{[4]}Al^{3+}$ for $^{[4]}Si^{4+}$ substitution is close to 70% (Table 2). With respect to phlogopite and Al-rich phlogopite, this substitution produces an increase in the volume of the tetrahedral sites (Fig. 1a, Tables 1 and 6) and a consequent increase in the thickness ($t_t$) of the sheet (Al-rich phlogopite: $2.250 \leq t_t \leq 2.259$ Å; clintonite: $2.309 \leq t_t \leq 2.329$ Å). Note that the thickness of the sheet in Al-rich phlogopite is midway between that in phlogopite and clintonite. The mean basal T-O bond distances ($<T\text{-}O>_{basal}$) and the apical T-O3 increase from phlogopite to clintonite (Fig. 1b). However, the T-O3 distance increases less rapidly than $<T\text{-}O>_{basal}$, and this generates regular and flatter tetrahedra (Fig. 1c): in the clintonite samples, edge length (ELD) and bond length (BLD) distortion (see Table 6) are less than 0.441 and 0.368%, respectively, and tetrahedral angle variance (TAV) varies between 0.0 and $(0.5°)^2$, whereas tetrahedral angle flattening ($\tau$) varies between 108.9 and 109.4°. The increase in the $<T\text{-}O>_{basal}$ value increases the lateral dimensions of the tetrahedral sheet. Thus, to link to the octahedral sheet, the tetrahedral sheet requires the tetrahedral rotation angle ($\alpha$) to approach its maximum value: $23.1 \leq \alpha \leq 24.9°$ (Fig. 1d).

In clintonite, the interlayer separation decreases on average by 0.6 Å with respect to the associated Al-rich phlogopite samples (Tables 1 and 6). Figure 1e also shows that, in brittle micas (clintonite and kinoshitalite) and in Ba-rich biotite, the reduction in the separation between two adjacent layers is inversely related to the $\alpha$ angle, whereas in true micas (phlogopite, biotite, Al-rich phlogopite, and ferriphlogopite), a different trend is found. The behavior of the brittle micas can be attributed not only to the interlayer cation size and charge (mostly Ca in clintonite and, K and Ba in kinoshitalite) but also to the increase in the negative charge of the basal O atom plane. Furthermore, as observed by MacKinney et al. (1988), the interlayer cation in F-rich clintonite can sink into the silicate ring, thereby further reducing the interlayer separation. (In our crystals, the high values of the $\alpha$ angle and the appreciable repulsion involving Ca and H cations reduced the Ca sinking into the cavity of the tetrahedral sheet.)

Figure 1f shows the relationships between the $\alpha$ angle and the dimensional misfit between the tetrahedral and octahedral sheets ($\Delta_{TM}$). Toraya (1981) pointed out that a linear relationship exists between the $\alpha$ angle and $\Delta_{TM}$: For true micas, linear regression gives $\alpha = 35.44\ \Delta_{TM} - 11.09$, whereas for synthetic germanium micas $\alpha = 12.58\ \Delta_{TM} + 4.30$. For the data reported in Figure 1f, we obtained the following linear regression: For true micas (phlogopite and biotite) $\alpha = 40.653\ \Delta_{TM} - 13.519$, $r = 0.955$; for brittle micas (clintonite and kinoshitalite) $\alpha = 19.773\ \Delta_{TM} - 0.709$, $r = 0.993$. It would therefore appear that, in brittle micas, a smaller variation in the $\alpha$ angle offsets a greater variation in $\Delta_{TM}$ than in the true micas. Therefore, in brittle micas, additional tetrahedral distortion parameters, such as a greater corrugation of the basal O atom plane, are required to fit the sheets.

### Octahedral sheet

In clintonite, the presence of $Al^{3+}$ in octahedral coordination reduces the dimensions of both M1 and M2 sites with respect to the $Al^{3+}$-rich phlogopite samples associated with them (clintonite: $2.029 \leq \langle M1\text{-}O\rangle \leq 2.042$ Å, $2.020\ \langle M2\text{-}O\rangle \leq 2.027$ Å; phlogopite: $2.066 \leq \langle M1\text{-}O\rangle \leq 2.072$ Å; $2.064 \leq \langle M2\text{-}O\rangle \leq 2.070$ Å; Tables 1 and 5), with a consequent decrease in the thickness of the sheet (Fig. 2a). However, for clintonite, volumes and flattening angles ($\Psi$) of the trans M1 octahedral site are greater than those of the cis M2 site (Table 6). This is the ''normal'' ordering scheme, i.e., low-charged, large cations preferentially occupy M1 (Bailey 1984; Guggenheim 1984). To characterize the external distortion and the central cation off-center shift of both M1 and M2 polyhedra more accurately, ELD (edge length distortion) and BLD (bond length distortion) parameters (Renner and Lehman 1986) were calculated. In general, the ELD values of the larger M1 site are slightly greater than those of the M2 site. This is consistent with the greater angle variance and angle flattening. Figure 2b shows that, in Al-rich phlogopite, the volumes and distortions of the M1 and M2 sites are generally comparable, whereas in clintonite the increase in the M1 site volume correlates with an increase in its distortion. Nevertheless, in both micas the BLD parameter is greater for the M1 than for the M2 site, which indicates that the M1 cations have a greater off-center shift. This result is explained by the variation of individual octahedral bond distances. These distances respond

←

**Figure 2.** (**a**) $^{[6]}Al^{3+} + {}^{[6]}Ti^{4+}$ vs. the octahedral sheet thickness; (**b**) ratio between M1 and M2 volumes vs. the ratio between unshared ($e_u$) and shared ($e_s$) octahedral edges of both M1 and M2 sites; (**c**) M1-O3 vs. T-O3 bond length; (**d**) M1-O4 vs. $\langle T\text{-}O\rangle_{basal}$; (**e**) M2-O4 vs. $\langle T\text{-}O\rangle_{basal}$; (**f**) M1-O4 vs. A-O4. Symbols: filled triangles = clintonite samples from this study; open triangles = clintonite from the literature (Joswig et al. 1986; MacKinney et al. 1988); filled circles = Al-rich phlogopite from the Predazzo-Monzoni area (Alietti et al. 1995).

differently to the increase in the lateral dimensions of the tetrahedral sheet; in particular, the M1-O3 distance decreases while M1-O4 and M2-O4 distances increase (Figs. 2c and 2d). Although the sum of bond distances [(T-O3) + (M1-O3)] remains virtually constant, M1-O3 and T-O3 distances are inversely linked; the T-O3 distance increases as a consequence of the Al for Si tetrahedral substitution, whereas distances M1-O3 (Fig. 2c) and M2-O3 decrease following the Al for Mg octahedral substitution. M1-O4 and M2-O4 bond distances are directly related to the increase in basal tetrahedral dimensions (Fig. 2d and 2e). Figure 2f shows that the increase in the M2-O4 (and also M1-O4) bond distance is inversely linked to the A-O4 distances. The lengthening of the M-O4 bond distances therefore requires an increase in the repulsion between the interlayer cation and $H^+$ associated with O4.

The compositional and structural characteristics of the clintonite samples from the Predazzo-Monzoni area and from the Adamello Massif suggest that they vary only slightly and differ little from that of the end-member. The limited extent of the exchange vector $^{[4]}Al_{-1}{}^{[6]}Mg_{-2}{}^{[4]}Si^{[6]}(Al,\square)$ can also be inferred, because the tetrahedral composition varies from $Si_{1.19}Al_{2.78}Fe_{0.03}$ to $Si_{1.28}Al_{2.70}Fe_{0.02}$. The natural clintonite samples in this study do not have as large an Al content as the synthetic samples (Olesch 1975). Although closely associated with phlogopite in some rock samples, the exchange vector $^{[4]}Al_{-1}{}^{[12]}Ca_{-1}{}^{[4]}Si{}^{[12]}K$ is unlikely in clintonite.

## Acknowledgments

We are grateful for the comments of two anonymous reviewers that stimulated us to reconsider some of our original conclusions. Financial support was provided by MURST and CNR of Italy. CNR is also acknowledged for the use of the ARL-SEMQ electron microprobe at the Department of Earth Sciences, Modena University.

## References cited

Alberti, A. and Gottardi, G. (1988) The determination of the Al-content in the tetrahedra of framework silicates. Zeitschrift für Kristallographie, 184, 49–61.

Alietti, E. (1996) Exchange vectors $K_{-1}Si_{-1}CaAl$ and $Si_{-1}Mg_{-1}Al_2$ in phlogopites and clintonites: crystal chemical implications. P.h.D. thesis abstract, Plinius, 15, 65–69.

Alietti, E., Brigatti, M.F., and Poppi, L. (1995) The crystal structure and chemistry of high aluminium phlogopite. Mineralogical Magazine, 59, 149–157.

Annersten, H. and Olesch, M. (1978) Distribution of ferrous and ferric iron in clintonite and the Mössbauer characteristic of ferric iron in tetrahedral coordination. Canadian Mineralogist, 16, 199–203.

Bailey, S.W. (1984) Crystal chemistry of the true micas. In Mineralogical Society of America Reviews in Mineralogy, 13, 13–60.

—— (1988) X-ray diffraction identification of the polytypes of mica, serpentine and chlorite. Clays and Clay Minerals, 36, 195–213.

Bigi, S., Brigatti, M.F., Mazzucchelli, M., and Rivalenti, G. (1993) Crystal chemical variations in Ba-rich biotites from gabbroic rocks of lower crust (Ivrea Zone, NW Italy). Contribution to Mineralogy and Petrology, 113, 87–99.

Brigatti, M.F. and Davoli, P. (1990) Crystal structure refinements of 1*M* plutonic biotites. American Mineralogist, 75, 305–313.

Brigatti, M.F. and Poppi, L. (1993) Crystal chemistry of Ba-rich trioctahedral micas 1*M*. European Journal of Mineralogy, 5, 857–871.

Brigatti, M.F., Galli, E., and Poppi, L. (1991) Effect of Ti substitution in biotite 1*M* crystal chemistry. American Mineralogist, 76, 1174–1183.

Brigatti, M.F., Medici, L., and Poppi, L. (1996) Refinement of the structure of natural ferriphlogopite. Clays and Clay Minerals, 44, 540–545.

Bucher-Nurminen, K. (1976) Occurrence and chemistry of xantophyllite in roof pendants of the Bergell granite, Sondrio, northern Italy. Schweizerische Mineralogische und Petrographische Mitteilungen, 56, 413–426.

Busing, W.R., Martin, K.O., and Levi, H.S. (1962) ORFLS, a Fortran crystallographic least-square program. U.S. National Technical Information Service, ORNL-TM-305.

Donnay, G., Morimoto, N., Takeda, H., and Donnay, D.H. (1964) Trioctahedral one-layer micas. 1. Crystal structure of a synthetic iron mica. Acta Crystallographica, 17, 1369–1373.

Foley, S.F. (1989) Experimental constraints on phlogopite chemistry in lamproites: 2. The effect of pressure-temperature variations. European Journal of Mineralogy, 2, 327–341.

Guggenheim, S. (1984) The brittle micas. In Mineralogical Society of America Reviews in Mineralogy, 13, 61–104.

Guggenheim, S. and Kato, T. (1984) Kinoshitalite and Mn phlogopites: Trial refinements in subgroup symmetry and futher refinement in ideal symmetry. Mineralogical Journal, 12, 1–5.

Hazen, R.M. and Burnham, C.W. (1973) The crystal structure of one-layer phlogopite and annite. American Mineralogist, 58, 889–900.

Hewitt, D.A. and Wones, D.R. (1975) Physical properties of some synthetic Fe-Mg-Al trioctahedral biotites. American Mineralogist, 60, 854–862.

Ibers, J.A. and Hamilton, W.C., Eds. (1974) International tables for X-ray crystallography, Vol. IV, p. 99–101. Kynoch, Birmingan, U.K.

Joswig, W. (1972) Neutronenbeugungsmessungen an einem 1*M*-phlogopit. Neues Jahrbuch für Mineralogie Monatshefte, 1–11.

Joswig, W., Amthaner, G., and Takéuchi, Y. (1986) Neutron diffraction and Mössbauer spectroscopic study of clintonite (xanthophyllite). American Mineralogist, 71, 1194–1197.

Kato, T., Miura, Y., Yoshii, M., and Maeda, K. (1979) The crystal structures of 1*M* kinoshitalite, a new barium brittle mica, and 1*M* manganese trioctahedral micas. Mineralogical Journal, 9, 392–408.

Lipson, H. and Cochran, W. (1953) The crystalline state. Vol. III. The determination of crystal structures. Bell and Sons, London.

Loewenstein, W. (1954) The distribution of aluminum in the tetrahedra of silicates and aluminates. American Mineralogist, 39, 92–96.

MacCauley, J.W., Newnham, R.E., and Gibbs, G.V. (1973) Crystal structure analysis of synthetic fluorophlogopite. American Mineralogist, 58, 249–254.

MacKinney, J.A., Mora, C.I., and Bailey, S.W. (1988) Structure and crystal chemistry of clintonite. American Mineralogist, 73, 365–375.

Marsh, R.E. (1986) Centrosymmetric or noncentrosymmetric? Acta Crystallographica, B42, 193–198.

Meyrowitz, R. (1970) New semi-microprocedure for determination of ferrous iron in refractory silicate minerals using a sodium metafluoborate decomposition. Analytical Chemistry, 42, 1110–1113.

Morandi, N., Nannetti, C., Pirani, R., and Resmi, U. (1984) La mica verde della roccia di contatto nell'area Predazzo-Monzoni. Rendiconti della Società Italiana di Mineralogia e Petrografia, 39, 677–693.

North, A.C.T., Phillips, D.C., and Mathews, F.S. (1968) A semi-empirical method of absorption correction. Acta Crystallographica, A24, 351–359.

Olesch, M. (1975) Synthesis and solid solubility of trioctahedral brittle micas in the system $CaO$-$MgO$-$Al_2O_3$-$SiO_2$-$H_2O$. American Mineralogist, 60, 188–199.

Olesch, M. and Seifert, F. (1976) Stability and phase relations of trioctahedral calcium brittle micas (clintonite group). Journal of Petrology, 17, parte 3, 291–314.

Pouchou, J.L. and Pichoir, F. (1991) Quantitative analyses of homogeneous or stratified microvolumes applying the model "PAP". In K.F.J. Heinrich and D.E. Newberry, Eds., Electron probe quantification, p. 31–75. Plenum, New York.

Renner, B. and Lehmann, G. (1986) Correlation of angular and bond length distortion in $TO_4$ units in crystals. Zeitschrift für Kristallographie, 175, 43–59.

Robinson, K., Gibbs, G.V., and Ribbe, P.H. (1971) Quadratic elongation, a quantitative measure of distortion in coordination polyhedra. Science, 172, 567–570.

Schomaker, V. and Marsh, R.E. (1979) Some comments on refinement in a space group of unnecessarily low symmetry. Acta Crystallographica, B35, 1933–1934.

Siemens (1993) XSCANS System—Technical reference. Siemens Analytical X-ray Instruments.

Takeda, H. and Morosin, B. (1975) Comparison of observed and predicted structural parameters of mica at high temperature. Acta Crystallographica, B31, 2444–2452.

Takéuchi, Y. (1966) Structural studies of brittle micas (I). The structure of xanthophyllite refined. Mineralogical Journal (Japan), 4, 424–437.

Takéuchi, Y. and Sadanaga, R. (1959) The crystal structure of xanthophyllite. Acta Crystallographica, 12, 945–946.

Tokonami, M. (1965) Atomic scattering factors for $O^{2-}$. Acta Crystallographica, 19, 486.

Toraya, H. (1981) Distorsions of octahedra and octahedral sheets in 1*M* micas and the relation to their stability. Zeitschrift für Kristallographie, 157, 173–190.

Ulmer, P. (1982) Monticellite-clintonite bearing assemblages at the southern border of the Adamello-Massif. Rendiconti Società Italiana di Mineralogia e Petrografia, 38, 617–628.

Ungaretti, L. (1980) Recent developments in X-ray single crystal diffractometry applied to the crystal chemical study of amphiboles. Godisnjac Iugoslavenskog Centraza Kristalograiju, 15, 29–65.

Ungaretti, L., Lombardo, B., Domeneghetti, M.C., and Rossi, G. (1983) Crystal-chemical evolution of amphiboles from eclogitised rocks of the Sesia-Lanzo Zone, Italian Western Alps. Bulletin de Minéralogie, 106, 645–672.

Manuscript received May 1, 1996
Manuscript accepted April 29, 1997